

Inverse Seesaw Neutrino Signatures at LHC and ILC

Arindam Das¹ and Nobuchika Okada²

*Department of Physics and Astronomy, University of Alabama,
Tuscaloosa, Alabama 35487, USA*

Abstract

We study the collider signature of pseudo-Dirac heavy neutrinos in the inverse seesaw scenario, where the heavy neutrinos with mass at the electroweak scale can have sizable mixings with the Standard Model neutrinos, while providing the tiny light neutrino masses by the inverse seesaw mechanism. Based on a simple, concrete model realizing the inverse seesaw, we fix the model parameters so as to reproduce the neutrino oscillation data and to satisfy other experimental constraints, assuming two typical flavor structures of the model and the different types of hierarchical light neutrino mass spectra. For completeness, we also consider a general parameterization for the model parameters by introducing an arbitrary orthogonal matrix, and the non-zero Dirac and Majorana phases. We perform parameter scan to identify an allowed parameter region which satisfies all experimental constraints. With the fixed parameters in this way, we analyze the heavy neutrino signal at the LHC through tri-lepton final states with large missing energy and at the ILC through a single lepton plus di-jet with large missing energy. We find that in some cases, the heavy neutrino signal can be observed with a large statistical significance via different flavor charged lepton final states.

¹adas8@ua.edu

²okadan@ua.edu

1 Introduction

The current experimental results on the neutrino oscillation phenomena [1], including the recent measurements of the so-called reactor angle [2, 3, 4, 5, 6], have established the existence of neutrino masses and flavor mixings, which require us to extend the Standard Model (SM). The seesaw extension of the SM [7] is probably the simplest idea for explaining the very small neutrino masses naturally, where the SM-singlet heavy right-handed Majorana neutrinos induce the dimension five operators leading to very small light Majorana neutrino masses (the seesaw mechanism [7]). The seesaw scale varies from the intermediate scale to the electroweak scale as we change the neutrino Dirac Yukawa coupling (Y_D) from the scale of top quark Yukawa coupling ($Y_D \sim 1$) to the scale of electron Yukawa coupling ($Y_D \sim 10^{-6}$).

In high energy collider experimental point of view, it is interesting if the heavy neutrino mass lies at the TeV scale or smaller, because such heavy neutrinos could be produced at high energy colliders, such as the Large Hadron Collider (LHC) and the International Linear Collider (ILC) being projected as energy frontier physics in the future. However, since the heavy neutrinos are singlet under the SM gauge group, they obtain the couplings with the weak gauge bosons only through the mixing via the Dirac Yukawa coupling. For the seesaw mechanism at the TeV scale or smaller, the Dirac Yukawa coupling is too small ($Y_D \sim 10^{-6} - 10^{-5}$) to produce the observable amount of the heavy neutrinos at the colliders.

There is another type of seesaw mechanism so-called the inverse seesaw [8], where the small neutrino mass is obtained by tiny lepton-number-violating parameters, rather than the suppression by the heavy neutrino mass scale in the ordinary seesaw mechanism. In the inverse seesaw scenario, the heavy neutrinos are pseudo-Dirac particles and their Dirac Yukawa couplings with the SM lepton doublets and the Higgs doublet can be even order one, while reproducing the small light neutrino masses. Thus, the heavy neutrinos in the inverse seesaw scenario can be produced at the high energy colliders through the sizable mixing with the SM neutrinos.

In this paper, we study the inverse seesaw scenario and the heavy neutrino signatures at the LHC and ILC. For the concreteness of our inverse seesaw scenario as well as the stability of the electroweak scale, we consider a simple realization of the inverse seesaw mechanism in the context of the next-to-minimal supersymmetric SM (NMSSM) proposed in [9]. The model parameters are fixed so as to reproduce the neutrino oscillation data as well as other experimental constraints such as precision measurements of the weak gauge boson decays and lepton-flavor-violating decays of charged leptons. We consider two typical cases in fitting neutrino oscillation data. One is that the flavor structure among light neutrinos originates from the flavor structure of the neutrino Dirac Yukawa couplings. In the other case, the Dirac Yukawa couplings are flavor-blind, and the flavor structure among light neutrinos is provided by the

lepton-number-violating parameters. Assuming the TeV scale mass for sparticles, we concentrate on the production of the heavy neutrinos with mass of $\mathcal{O}(100)$ GeV at the LHC and ILC, and calculate the number of signal events. The heavy neutrino signals depend on the origin of the flavor structure in the model and the types of the hierarchical light neutrino mass spectra. We find that in some cases, the signal of the heavy neutrino productions can be observed in the future collider experiments with a large statistical significance for the final states with different charged lepton flavors.

This paper is organized as follows. In Sec. 2, we introduce a model for the inverse seesaw in the context of NMSSM. In Sec. 3 we give the explicit formulas of the heavy neutrino production cross sections at the LHC and ILC and of the partial decay widths, which are used in our numerical analysis. In Sec. 4, we first fix the model parameters in simple parameterizations so as to satisfy the experimental constraints, assuming two typical flavor structures of our model and two types of hierarchical neutrino mass spectra. For completeness, we also consider a general parameterization of the neutrino Dirac mass matrix. In Sec 5, the signal of the heavy neutrinos at the LHC and ILC are investigated. For the general parameterization, we perform parameter scan to identify the parameter region to satisfy all experimental constraints, for which we examine how much the heavy neutrino signal is enhanced. Sec. 6 is devoted for conclusions.

2 Inverse Seesaw in NMSSM

As a simple realization of the inverse seesaw mechanism, we consider an extension of the NMSSM [10]. In the NMSSM, we introduce one gauge singlet chiral superfield S with even Z_2 matter parity through the following superpotential terms:

$$W \supset \lambda S H_u H_d + \frac{\kappa}{3} S^3 \quad (1)$$

where λ and κ are the dimensionless constants, H_u , H_d are the MSSM Higgs doublets. We assume that the hidden sector breaks supersymmetry (SUSY) and induces soft SUSY breaking terms for the MSSM scalars and gauginos at the TeV scale, by which the scalar S and the MSSM Higgs doublets develop the vacuum expectation values (VEVs). The VEV of S generates the MSSM μ term: $\mu = \lambda \langle S \rangle$.

We extend the NMSSM by introducing new particles and a discrete Z_3 symmetry [9]. The charge assignments for particles relevant to the inverse seesaw mechanism are shown in Table 1. Here, N_j^c and N_j are the MSSM singlet particles, heavy neutrinos of j -th generation, and $\omega = e^{i2\pi/3}$. There are several possibilities for the Z_3 charge assignments, and see [9] for complete lists.

	SU(2)	U(1) _Y	Z ₃	Z ₂
L	2	-1/2	1	-
E^c	1	+1	ω^2	-
H_u	2	+1/2	ω	+
H_d	2	-1/2	ω	+
S	1	0	ω	+
N_j^c	1	0	ω^2	-
N_j	1	0	ω	-

Table 1: The charge assignments of the NMSSM superfields.

The renormalizable superpotential involving the new particles and being consistent with all the symmetries is given by

$$W \supset Y_{ij} L_i H_u N_j^c + \frac{(\lambda_N)_{ij}}{2} S N_i N_j + m_{ii} N_i N_i^c. \quad (2)$$

Without loss of generality, we have worked out in the basis where the charged lepton Yukawa matrix and m are diagonalized. When the VEVs of S and H_u are developed, we rewrite the superpotential as

$$W \supset \nu^T m_D N^c + \frac{1}{2} N^T \mu N + N^T m N^c, \quad (3)$$

where we have used the matrix notation for generation indices, ν is the MSSM neutrino chiral superfield, $m_D = Y v \sin \beta / \sqrt{2}$ with $v = 246$ GeV is the neutrino Dirac mass matrix, and $\mu = \lambda_N \langle S \rangle$. For m larger than the electroweak scale, we integrate out the heavy fields N^c and N under the SUSY vacuum conditions,

$$\begin{aligned} \frac{\partial W}{\partial N} = 0 &\rightarrow N^c = -m^{-1} \mu N, \\ \frac{\partial W}{\partial N^c} = 0 &\rightarrow N = -(m_D m^{-1})^T \nu, \end{aligned} \quad (4)$$

and we arrive at the effective superpotential at low energies,

$$W_{\text{eff}} = \frac{1}{2} \nu^T [(m_D m^{-1}) \mu (m_D m^{-1})^T] \nu. \quad (5)$$

Note that the light Majorana neutrino mass matrix, $m_\nu = (m_D m^{-1}) \mu (m_D m^{-1})^T$, is proportional to μ , so that tiny neutrino masses can be realized by a small μ even for both m and m_D being the electroweak scale. This is the inverse seesaw mechanism, where the tiny neutrino mass corresponds to the breaking of the lepton number by the tiny μ values.

Note that the heavy fields being integrated out also have an impact on the Kähler potential. Substituting the SUSY vacuum conditions into the canonical Kähler potential for the heavy fields, $\int d^4\theta(N^\dagger N + N^{c\dagger}N^c)$, we obtain

$$\mathcal{K}_{\text{eff}} = \nu^\dagger [(m_D m^{-1})^* (m_D m^{-1})^T] \nu + \dots, \quad (6)$$

where the ellipsis denote higher order terms. Following the electroweak symmetry breaking, this dimension six operator induces flavor-dependent corrections to the kinetic terms of the left-handed neutrinos [11].

Assuming $m_D m^{-1} \ll 1$, we can express the flavor eigenstates (ν) of the light Majorana neutrinos in terms of the mass eigenstates of the light (ν_m) and heavy (N_m) Majorana neutrinos such as

$$\nu \simeq \mathcal{N}\nu_m + \mathcal{R}N_m, \quad (7)$$

where

$$\mathcal{R} = m_D m^{-1}, \quad \mathcal{N} = \left(1 - \frac{1}{2}\epsilon\right) U_{MNS} \quad (8)$$

with $\epsilon = \mathcal{R}^* \mathcal{R}^T$, and U_{MNS} is the usual neutrino mixing matrix by which the mass matrix m_ν is diagonalized as

$$U_{MNS}^T m_\nu U_{MNS} = \text{diag}(m_1, m_2, m_3). \quad (9)$$

In the presence of ϵ , the mixing matrix \mathcal{N} is not unitary. Using the mass eigenstates, the charged current interaction in the Standard Model is given by

$$\mathcal{L}_{CC} = -\frac{g}{\sqrt{2}} W_\mu \bar{e} \gamma^\mu P_L (\mathcal{N}\nu_m + \mathcal{R}N_m) + h.c., \quad (10)$$

where e denotes the three generations of the charged leptons in the vector form, and $P_L = \frac{1}{2}(1 - \gamma_5)$ is the projection operator. Similarly, the neutral current interaction is given by

$$\mathcal{L}_{NC} = -\frac{g}{2c_w} Z_\mu \left[\bar{\nu}_m \gamma^\mu P_L (\mathcal{N}^\dagger \mathcal{N}) \nu_m + \overline{N_m} \gamma^\mu P_L (\mathcal{R}^\dagger \mathcal{R}) N_m + \{ \bar{\nu}_m \gamma^\mu P_L (\mathcal{N}^\dagger \mathcal{R}) N_m + h.c. \} \right], \quad (11)$$

where $c_w = \cos \theta_w$ is the weak mixing angle. Because of non-unitarity of the matrix \mathcal{N} , $\mathcal{N}^\dagger \mathcal{N} \neq 1$ and the flavor-changing neutral current occurs.

3 Productions and decays of heavy neutrinos at colliders

In the previous section, we have found the charged and neutral current interactions involving the heavy neutrinos. For detailed analysis, we need the information of the mixing matrices,

\mathcal{N} and \mathcal{R} . In the next section, we will fix all the elements of the matrices by considering the current experimental results. Before the analysis for fixing the parameters, in this section we give the formulas for the production cross sections and the partial decay widths of the heavy neutrinos in the limit of one generation and $\mathcal{N} = \mathcal{R} = 1$.

3.1 Production cross section at LHC

At the LHC, the heavy neutrinos can be produced through the charged current interactions by the s -channel exchange of the W boson. The main production process at the parton level is $u\bar{d} \rightarrow e^+ N_1$ (and $\bar{u}d \rightarrow e^- \bar{N}_1$) and the differential cross section is found to be

$$\frac{d\hat{\sigma}_{LHC}}{d\cos\theta} = (3.89 \times 10^8 \text{ pb}) \times \frac{\beta}{32\pi\hat{s}} \frac{\hat{s} + M^2}{\hat{s}} \left(\frac{1}{2}\right)^2 3 \left(\frac{1}{3}\right)^2 \frac{g^4 (\hat{s}^2 - M^4)(2 + \beta \cos^2 \theta)}{4 (\hat{s} - m_W^2)^2 + m_W^2 \Gamma_W^2}, \quad (12)$$

where $\sqrt{\hat{s}}$ is the center-of-mass energy of the colliding partons, M is the mass of N_1 , and $\beta = (\hat{s} - M^2)/(\hat{s} + M^2)$.

The total production cross section at the LHC is given by

$$\begin{aligned} \sigma_{LHC} &= \int d\sqrt{\hat{s}} \int d\cos\theta \int_{\hat{s}/E_{CMS}^2}^1 dx \frac{4\hat{s}}{xE_{CMS}^2} f_u(x, Q) f_{\bar{d}}\left(\frac{\hat{s}}{xE_{CMS}}, Q\right) \frac{d\hat{\sigma}_{LHC}}{d\cos\theta} \\ &+ (u \rightarrow \bar{u}, \bar{d} \rightarrow d), \end{aligned} \quad (13)$$

where we have taken $E_{CMS} = 14$ TeV for the center-of-mass energy of the LHC. In our numerical analysis, we employ CTEQ5M [12] for the parton distribution functions for u -quark (f_u) and \bar{d} -quark ($f_{\bar{d}}$) with the factorization scale $Q = \sqrt{\hat{s}}$. The total cross section as a function of M is depicted in Fig. 1. Since we have fixed $\mathcal{N} = \mathcal{R} = 1$ in this analysis, the resultant cross section shown in Fig. 1 corresponds to the maximum values for a fixed M .

There are three main modes for the heavy neutrino decays: $N_1 \rightarrow e^- W^+$, $\nu_1 Z$, $\nu_1 h$. The corresponding partial decay widths are respectively given by

$$\begin{aligned} \Gamma(N_1 \rightarrow e^- W^+) &= \frac{g^2}{64\pi} \frac{(M^2 - m_W^2)^2 (M^2 + 2m_W^2)}{M^3 m_W^2}, \\ \Gamma(N_1 \rightarrow \nu_1 Z) &= \frac{g^2}{128\pi c_w^2} \frac{(M^2 - m_Z^2)^2 (M^2 + 2m_Z^2)}{M^3 m_Z^2}, \\ \Gamma(N_1 \rightarrow \nu_1 h) &= \frac{(M^2 - m_h^2)^2}{32\pi M} \left(\frac{1}{v \sin\beta}\right)^2. \end{aligned} \quad (14)$$

The long-sought Higgs boson is finally discovered by the ATLAS [13] and the CMS [14] collaborations at the LHC. According to the discovery, we use $m_h = 125.3$ GeV [14] in the following analysis. Our results are almost independent of the choice of the Higgs boson mass in the range of 125 – 126 GeV.

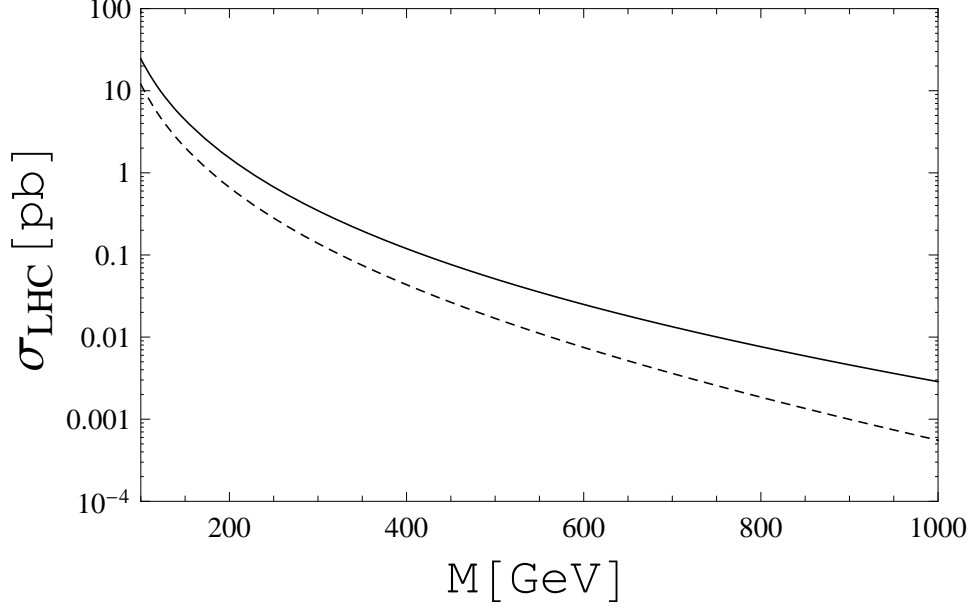


Figure 1: The total production cross section of the heavy neutrino as a function of its mass at the LHC with $\sqrt{s} = 14$ TeV (solid line). As a reference, the production cross section at the LHC with $\sqrt{s} = 8$ TeV is also plotted (dashed line).

3.2 Production cross section at ILC

The ILC can produce the heavy neutrino in the process $e^+e^- \rightarrow \bar{\nu}_1 N_1$ through t and s -channels exchanging the W and Z bosons, respectively. The total differential production cross section for this process is calculated as

$$\begin{aligned}
\frac{d\sigma_{ILC}}{d\cos\theta} &= (3.89 \times 10^8 \text{ pb}) \times \frac{\beta}{32\pi s} \frac{s + M^2}{s} \left(\frac{1}{2}\right)^2 \\
&\times \left[\frac{16C_1^2 C_2^2 (s^2 - M^4) (1 + \cos\theta)(1 + \beta \cos\theta)}{(M^2 - \frac{s-M^2}{2}(1 - \beta \cos\theta) - m_W^2)^2 + m_W^2 \Gamma_W^2} \right. \\
&+ \frac{(4(C_{A_e}^2 + C_{V_e}^2)(C_{A_\nu}^2 + C_{V_\nu}^2)(1 + \beta \cos^2\theta) + 16C_{A_e} C_{V_e} C_{A_\nu} C_{V_\nu} (1 + \beta) \cos\theta) (s^2 - M^4)}{(s - m_Z^2)^2 + m_Z^2 \Gamma_Z^2} \\
&- 32C_1^2 C_{A_e}^2 (s^2 - M^4)(1 + \cos\theta)(1 + \beta \cos\theta) \\
&\left. \times \frac{\left(M^2 - \frac{s-M^2}{2}(1 - \beta \cos\theta) - m_W^2\right) (s - m_Z^2) + m_W m_Z \Gamma_W \Gamma_Z}{\left((M^2 - \frac{s-M^2}{2}(1 - \beta \cos\theta) - m_W^2)^2 + m_W^2 \Gamma_W^2\right) \left((s - m_Z^2)^2 + m_Z^2 \Gamma_Z^2\right)} \right], \quad (15)
\end{aligned}$$

where $\beta = (s - M^2)/(s + M^2)$,

$$\begin{aligned} C_1 = -C_2 &= \frac{g}{2\sqrt{2}}, \quad C_{A\nu} = C_{V\nu} = \frac{g}{4\cos\theta_w}, \\ C_{Ae} &= \frac{g}{2\cos\theta_w} \left(-\frac{1}{2} + 2\sin^2\theta_w \right), \quad C_{Ve} = -\frac{g}{4\cos\theta_w}. \end{aligned} \quad (16)$$

The total production cross section for the process $e^+e^- \rightarrow \bar{\nu}_1 N_1$ for the ILC with $\sqrt{s} = 500$ GeV and 1 TeV, respectively, are shown in Fig. 2. Since we have fixed $\mathcal{N} = \mathcal{R} = 1$ in this analysis, the resultant cross section shown in Fig. 2 corresponds to the maximum values for a fixed M .

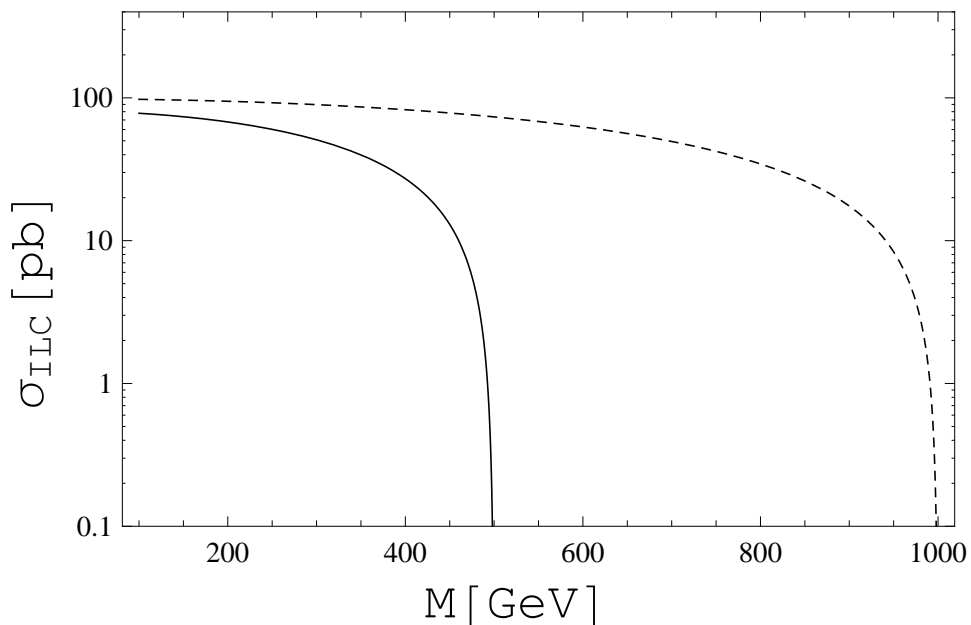


Figure 2: The total production cross section of the process $e^+e^- \rightarrow \bar{\nu}_1 N_1$ at the ILC with $\sqrt{s} = 500$ GeV (solid line) and $\sqrt{s} = 1$ TeV (dashed line).

4 Fixing the matrices \mathcal{N} and \mathcal{R}

4.1 Simple parameterizations

The elements of the matrices \mathcal{N} and \mathcal{R} are constrained by the experimental results [15, 16, 17]. We begin with the current neutrino oscillation data. Recently non-zero reactor neutrino angle θ_{13} has been observed in several experiments, such as T2K [2], MINOS [3], Double CHOOZ [4], Daya Bay [5] and RENO [6], and their results are consistent with each other. Together with

other oscillation data, all neutrino oscillation parameters except the Dirac CP-phase, two mass squared differences and three mixing angles have been measured in some precision. By using the data, we fix the neutrino mixing matrix elements. In the following analysis, we adopt $\sin^2 2\theta_{13} = 0.092$ [5] along with the other oscillation data: $\sin^2 2\theta_{12} = 0.87$, $\sin^2 2\theta_{23} = 1.0$, $\Delta m_{12}^2 = m_2^2 - m_1^2 = 7.6 \times 10^{-5} \text{ eV}^2$, and $\Delta m_{23}^2 = |m_3^2 - m_2^2| = 2.4 \times 10^{-3} \text{ eV}^2$. Then, the numerical values of neutrino mixing matrix elements are explicitly given by

$$U_{MNS} = \begin{pmatrix} 0.815 & 0.559 & 0.153 \\ -0.489 & 0.522 & 0.699 \\ 0.310 & -0.645 & 0.699 \end{pmatrix}, \quad (17)$$

where we have fixed all the CP-phases to be zero, for simplicity. We will discuss a general parameterization including all CP-phases as well as an arbitrary orthogonal matrix in the next subsection.

For the neutrino mass spectrum, we consider both the normal hierarchy (NH) and the inverted hierarchy (IH). The lightest mass eigenstate is assumed to be very light and its mass is approximated as 0. Thus, in the NH case, the diagonal mass matrix is given by

$$D_{NH} = \text{diag} \left(0, \sqrt{\Delta m_{12}^2}, \sqrt{\Delta m_{12}^2 + \Delta m_{23}^2} \right), \quad (18)$$

while in the IH case

$$D_{IH} = \text{diag} \left(\sqrt{\Delta m_{23}^2 - \Delta m_{12}^2}, \sqrt{\Delta m_{23}^2}, 0 \right). \quad (19)$$

In order to make our discussion simple, we assume the degeneracy of the heavy neutrinos in mass such as $m = M\mathbf{1}$ with the unit matrix $\mathbf{1}$, so that the neutrino mass matrix is simplified as

$$m_\nu = \mathcal{R}\mu\mathcal{R}^T = \frac{1}{M^2}m_D\mu m_D^T. \quad (20)$$

Moreover we consider two typical cases for the flavor structure of the model: (i) μ is also proportional to the unit matrix, $\mu \rightarrow \mu\mathbf{1}$. In this case, the flavor structure of m_ν is provided by a non-diagonal m_D . We call this case Flavor Non-Diagonal (FND) case. (ii) The other case is what we call Flavor Diagonal (FD) case, where m_D is proportional to the unit matrix, $m_D \rightarrow m_D\mathbf{1}$ and thus the flavor structure is encoded in the 3×3 matrix μ .

In the FND case, we consider two generations of N_j and N_j^c with $j = 1, 2$, so that

$$m_\nu = \frac{\mu}{M^2}m_D m_D^T = U_{MNS}^* D_{NH/IH} U_{MNS}^\dagger. \quad (21)$$

From this formula, we parameterize the neutrino Dirac mass matrix as

$$m_D = \frac{M}{\sqrt{\mu}} U_{MNS}^* \sqrt{D_{NH/IH}}, \quad (22)$$

where the matrices denoted as $\sqrt{D_{NH/IH}}$ are defined as

$$\sqrt{D_{NH}} = \begin{pmatrix} 0 & 0 \\ (\Delta m_{12}^2)^{\frac{1}{4}} & 0 \\ 0 & (\Delta m_{23}^2 + \Delta m_{12}^2)^{\frac{1}{4}} \end{pmatrix}, \quad \sqrt{D_{IH}} = \begin{pmatrix} (\Delta m_{23}^2 - \Delta m_{12}^2)^{\frac{1}{4}} & 0 \\ 0 & (\Delta m_{23}^2)^{\frac{1}{4}} \\ 0 & 0 \end{pmatrix}. \quad (23)$$

Note that in the case with two generations of N_j and N_j^c , the lightest mass eigenvalue is exactly 0. On the other hand, in the FD case, we have

$$m_\nu = \left(\frac{m_D}{M}\right)^2 \mu = U_{MNS}^* D_{NH/IH} U_{MNS}^\dagger. \quad (24)$$

Due to its non-unitarity, the elements of the mixing matrix \mathcal{N} are severely constrained by the combined data from neutrino oscillation experiments, the precision measurement of weak boson decays, and the lepton-flavor-violating decays of charged leptons [15, 16, 17]. We update the results by using more recent data on the lepton-flavor-violating decays [18, 19, 20]:

$$|\mathcal{N}\mathcal{N}^\dagger| = \begin{pmatrix} 0.994 \pm 0.00625 & 1.499 \times 10^{-5} & 8.764 \times 10^{-3} \\ 1.499 \times 10^{-5} & 0.995 \pm 0.00625 & 1.046 \times 10^{-2} \\ 8.764 \times 10^{-3} & 1.046 \times 10^{-2} & 0.995 \pm 0.00625 \end{pmatrix}. \quad (25)$$

Since $\mathcal{N}\mathcal{N}^\dagger \simeq \mathbf{1} - \epsilon$, we have the constraints on ϵ such that

$$|\epsilon| = \begin{pmatrix} 0.006 \pm 0.00625 & < 1.499 \times 10^{-5} & < 8.764 \times 10^{-3} \\ < 1.5 \times 10^{-5} & 0.005 \pm 0.00625 & < 1.046 \times 10^{-2} \\ < 8.76356 \times 10^{-3} & < 1.046 \times 10^{-2} & 0.005 \pm 0.00625 \end{pmatrix}. \quad (26)$$

The most stringent bound is given by the (1, 2) element which is from the constraint on the lepton-flavor-violating muon decay $\mu \rightarrow e\gamma$ ¹. For the FND case, we describe ϵ as

$$\epsilon = \frac{1}{M^2} m_D m_D^T = \frac{1}{\mu} U_{MNS} D_{NH/IH} U_{MNS}^T, \quad (27)$$

and determine the minimum μ value (μ_{min}) so as to give $\epsilon_{12} = 1.5 \times 10^{-5}$ using the oscillation data in Eqs. (17), (18) and (19). We have found $\mu_{min} = 525$ eV and 329 eV for the NH and IH cases, respectively. Here we have used the fact that all parameters are real according to our assumption. In this way, we can completely determine the mixing matrix \mathcal{R} and \mathcal{N} from Eq. (22) by taking $\mu = \mu_{min}$, which optimizes the production cross sections of the heavy neutrinos at the LHC and ILC. For the FD case, we simply take $\epsilon = (m_D/M)^2 \mathbf{1} = 0.012251$ (95.5% CL).

¹ It has been pointed out [22, 23] that in the SUSY inverse seesaw model, sparticle Z-penguin contributions can dominate the lepton-flavor-violating processes, independently of sparticle mass spectrum. According to the analysis in Ref. [23], we have found that the constraint from $\mu - e$ conversion process is more severe than the one from the $\mu \rightarrow e\gamma$ process for $M > 335$ GeV. Since we will focus on $M = 100 - 150$ GeV in the following analysis, we use the value of μ_{min} determined from the muon decay constraints.

4.2 General parameterization

For completeness, we also consider a general parameterization for the neutrino Dirac mass matrix for the FND case. From the inverse seesaw formula,

$$m_\nu = \mu \mathcal{R} \mathcal{R}^T = \frac{\mu}{M^2} m_D m_D^T = U_{MNS}^* D_{NH/IH} U_{MNS}^\dagger, \quad (28)$$

we can generally parameterize \mathcal{R} as

$$\mathcal{R}(\delta, \rho, x, y) = \frac{1}{\sqrt{\mu}} U_{MNS}^* \sqrt{D_{NH/IH}} O, \quad (29)$$

where O is a general orthogonal matrix expressed as

$$O = \begin{pmatrix} \cos \alpha & \sin \alpha \\ -\sin \alpha & \cos \alpha \end{pmatrix} = \begin{pmatrix} \cosh y & i \sinh y \\ -i \sinh y & \cosh y \end{pmatrix} \begin{pmatrix} \cos x & \sin x \\ -\sin x & \cosh x \end{pmatrix}, \quad (30)$$

with a complex number $\alpha = x + iy$, and the general form of the neutrino mixing matrix,

$$U_{MNS} = \begin{pmatrix} C_{12}C_{13} & S_{12}C_{13} & S_{13}e^{i\delta} \\ -S_{12}C_{23} - C_{12}S_{23}S_{13}e^{i\delta} & C_{12}C_{23} - S_{12}S_{23}S_{13}e^{i\delta} & S_{23}C_{13} \\ S_{12}S_{23} - C_{12}C_{23}S_{13}e^{i\delta} & -C_{12}S_{23} - S_{12}C_{23}S_{13}e^{i\delta} & C_{23}C_{13} \end{pmatrix} \begin{pmatrix} 1 & 0 & 0 \\ 0 & e^{i\rho} & 0 \\ 0 & 0 & 1 \end{pmatrix}. \quad (31)$$

Here, $C_{ij} = \cos \theta_{ij}$, $S_{ij} = \sin \theta_{ij}$, δ is the Dirac phase and ρ is the Majorana phase. Thus, in this general parameterization, we have

$$\epsilon(\delta, \rho, y) = \mathcal{R}^* \mathcal{R}^T = \frac{1}{\mu} U_{MNS} \sqrt{D_{NH/IH}} O^* O^T \sqrt{D_{NH/IH}}^T U_{MNS}^\dagger. \quad (32)$$

Note that

$$O^* O^T = \begin{pmatrix} \cosh^2 y + \sinh^2 y & -2i \cosh y \sinh y \\ 2i \cosh y \sinh y & \cosh^2 y + \sinh^2 y \end{pmatrix} \quad (33)$$

is independent of x , and hence the ϵ -matrix is a function of δ , ρ and y .

In the next section, we perform a parameter scan under the experimental constraints and identify an allowed region for the parameter set $\{\delta, \rho, y\}$. Then, we calculate the heavy neutrino production cross section for the parameter set and examine how much the production cross section is enhanced, satisfying the experimental constrains.

5 Collider signatures of heavy neutrinos

Let us now investigate the collider signatures of the heavy neutrinos with the information of \mathcal{R} and \mathcal{N} determined by the previous sections. In Sec. 3, we have already given the formulas used in our analysis in the limit of $\mathcal{R} = \mathcal{N} = 1$. It is easy to generalize the formulas with the

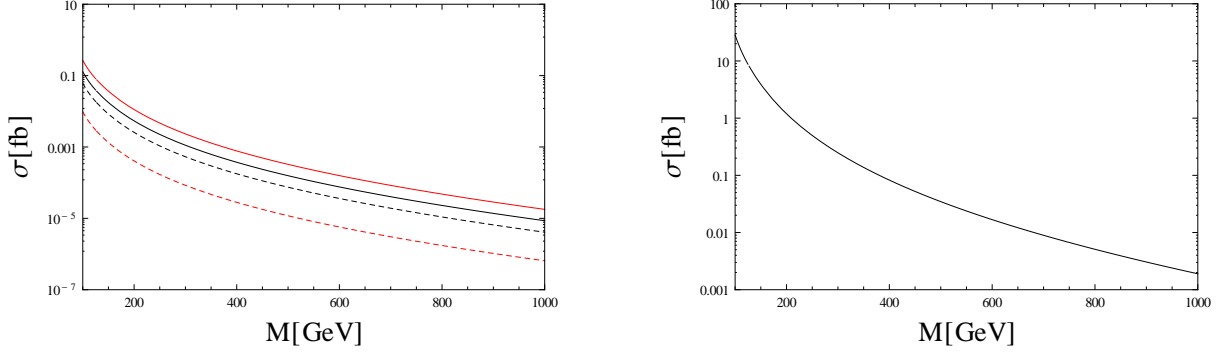


Figure 3: Signal cross sections providing the tri-lepton final states for the FND (left panel) and FD (right panel) cases, at the LHC with $\sqrt{s} = 14$ TeV.

concrete \mathcal{R} and \mathcal{N} . The production cross section of the i -th generation heavy neutrino at the LHC, through the process $q\bar{q}' \rightarrow \ell N_i$ ($u\bar{d} \rightarrow \ell_\alpha^+ N_i$ and $\bar{u}d \rightarrow \ell_\alpha^- \bar{N}_i$) is given by

$$\sigma(q\bar{q}' \rightarrow \ell_\alpha N_i) = \sigma_{LHC} |\mathcal{R}_{\alpha i}|^2, \quad (34)$$

where σ_{LHC} is the cross section given in Eq. (13). Similarly, the production cross section at the ILC is

$$\sigma(e^+e^- \rightarrow \bar{\nu}_\alpha N_i) = \sigma_{ILC} |\mathcal{R}_{\alpha i}|^2, \quad (35)$$

where σ_{ILC} is given in Eq. (15), and we have used the approximation $\mathcal{N}^\dagger \mathcal{R} \simeq U_{MNS}^\dagger \mathcal{R}$ because $|\epsilon_{\alpha\beta}| \ll 1$ as discussed in the previous section. The partial decay widths for the process $N_i \rightarrow \ell_\alpha^- W^+ / \nu_\alpha Z / \nu_\alpha h$ are obtained by multiplying Eq. (14) and the factor $|\mathcal{R}_{\alpha i}|^2$ together.

5.1 Heavy neutrino signal at LHC with the simple parameterizations

As has been studied in Ref. [21] (see also [24] for the studies on the left-right symmetric model), the most promising signal of the heavy neutrino productions at the LHC is obtained by the final state with three charged leptons ($\ell^\pm \ell^\pm \ell^\mp$ with the total charge ± 1) through the process $q\bar{q}' \rightarrow N \ell^\pm$ followed by $N \rightarrow \ell^\pm W^\mp$ and $W^\mp \rightarrow \ell^\mp \nu$. In this work, detailed studies have been performed for the signal of the heavy neutrino with a 100 GeV mass, which couples with either the electron or the muon. The events were pre-selected for two like-sign charged leptons (ee or $\mu\mu$) to have transverse momentum $p_T > 30$ GeV. The decay mode, $N \rightarrow \nu Z$, followed by $Z \rightarrow \ell^+ \ell^-$ is rejected by a cut for the invariant mass of the charge neutral di-lepton. After elaborate selections, it has been concluded [21] that the heavy neutrino coupling to the muon could be observed at the LHC through the tri-lepton final states.

	ee	$\mu\mu$
FND (NH)	0.254	1.61
FND (IH)	7.00	3.38
FD	58.7	56.2
SM background	116.4	45.6

Table 2: Number of events at the LHC with $\sqrt{s} = 14$ TeV and 30 fb^{-1} luminosity, for the heavy neutrino mass $M = 100$ GeV.

In our analysis, we follow the procedure in [21]. Since we are considering the general case with \mathcal{R} and \mathcal{N} consistent with the updated experimental data, the production cross sections of the heavy neutrinos are different from the ones in [21]. Fig. 3 shows the signal cross section providing tri-lepton final states with ee or $\mu\mu$ for the FND (left) and FD (right) cases, as a function of the heavy neutrino mass. In the left panel, the dashed and solid lines correspond to the NH and IH cases, respectively. The upper solid (dashed) line shows the cross sections with ee ($\mu\mu$).

We adopt the same efficiency for the signal events and the SM background events which was found in [21]. The number of events for tri-lepton final states with ee and $\mu\mu$, respectively, are listed on Table 2, for the luminosity 30 fb^{-1} . Unfortunately, the number of events for the FND case are found to be too small. This is because the component of \mathcal{R} is severely constrained to be small by the current experiments. On the other hand, the FD case results the large number of signal events specially in the $\mu\mu$ case with a significance of more than $5\text{-}\sigma$. If we naively estimate the significance by S/\sqrt{B} , the luminosity of 25 fb^{-1} (11 fb^{-1}) is required to achieve $5\text{-}\sigma$ significance for the ($\mu\mu$) final states.

5.2 Heavy neutrino signal at ILC with the simple parameterizations

The signature of heavy neutrinos at the ILC has been studied in detail based on the realistic Monte Carlo simulations in [25]. In the studies, a five-dimensional model with bulk right-handed neutrinos [26] is considered and its 4-dimensional effective theory provides the Kaluza-Klein tower of the heavy neutrinos having sizable coupling to the weak gauge bosons through mixings with the SM light neutrinos. This structure of the couplings between the heavy neutrinos and the SM particles in the five-dimensional model is similar to the one in our inverse seesaw model. Thus, we apply the results in [25], in particular, the signal and background selection procedure to our model.

According to [25], we focus on the two-jets and one isolated lepton signal with large missing energy at the ILC: $e^+e^- \rightarrow \nu N$, followed by the decays $N \rightarrow \ell W$ and $W \rightarrow q\bar{q}'$, through which

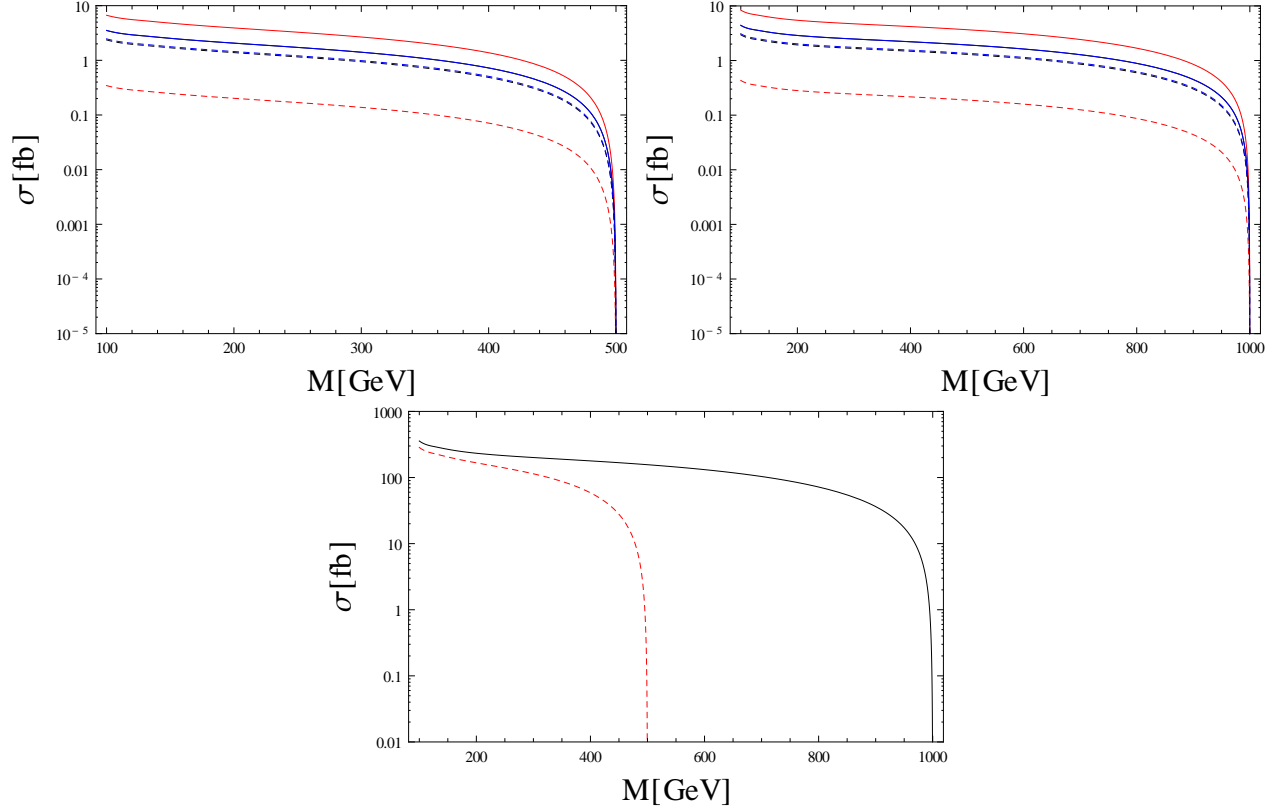


Figure 4: The production cross sections for the process $e^+e^- \rightarrow \nu N$, followed by the decays $N \rightarrow \ell W$ ($\ell = e, \mu, \tau$) and $W \rightarrow q\bar{q}'$, as a function of the heavy neutrino mass. The upper-left panel shows the results for the FND case with $\sqrt{s} = 500$ GeV. The upper-right panel is the same as the upper-left panel but for the case with $\sqrt{s} = 1$ TeV. The results for the FD case are shown in the lower panel for $\sqrt{s} = 500$ GeV (solid) and $\sqrt{s} = 1$ TeV (dashed), respectively.

the heavy neutrino production cross sections and the heavy neutrino mass can be reconstructed. The production cross sections for the process $e^+e^- \rightarrow \nu N$, followed by the decays $N \rightarrow \ell W$ ($\ell = e, \mu, \tau$) and $W \rightarrow q\bar{q}'$, as a function of the heavy neutrino mass are depicted in Fig. 4. The upper-left panel shows the results for the FND case with $\sqrt{s} = 500$ GeV. The dashed lines from top to bottom denote the signal cross sections for $\ell = \tau, \mu$ and e , respectively, in the NH case. The two lines corresponding to $\ell = \tau$ and μ are well-overlapping. The solid lines from top to bottom denote the signal cross sections for $\ell = e, \tau$ and μ , respectively, in the IH case. The two dashed lines corresponding to $\ell = \mu$ and τ are well-overlapping. The upper-right panel is the same as the upper-left panel but for the case with $\sqrt{s} = 1$ TeV. The results for the FD case are shown in the lower panel for $\sqrt{s} = 500$ GeV (dashed) and $\sqrt{s} = 1$ TeV (solid), respectively. Here ℓ is either e, μ or τ .

For the ILC with $\sqrt{s} = 500$ GeV and the luminosity $\mathcal{L} = 500 \text{ fb}^{-1}$, the signal and background

events are listed on Table 2, Here, the final state of one electron and two jets with missing energy from anti-neutrinos is considered, and we have adopted the efficiencies found in [25], for $M = 150$ GeV. The main backgrounds are $e\nu W \rightarrow e\nu q\bar{q}$ and $WW \rightarrow \ell\nu q\bar{q}$, which are dramatically reduced by the selection using an isolated-electron track with a requirement of its energy range, $10 \text{ GeV} \leq E_e \leq 200 \text{ GeV}$, the requirement of the reconstructed di-jet mass to be consistent with W hypothesis etc (see [25] for details). The signal and background events for $\sqrt{s} = 1$ TeV and the same luminosity $\mathcal{L} = 500 \text{ fb}^{-1}$ are listed on Table 3. For completeness, we have also listed the signal events (without cuts) for the case of $\ell = \mu$ and τ .

	Events before cuts	Events after cuts
FND (NH)	123.7	84.04
FND (IH)	2397	1363
FD	102210	69189.7
SM background	3210500	23346
FND (NH, $\ell = \mu$)	847.5	
FND (NH, $\ell = \tau$)	887.0	
FND (IH, $\ell = \mu$)	1261	
FND (IH, $\ell = \tau$)	1266	

Table 3: The number of events at the ILC with $\sqrt{s} = 500$ GeV and the luminosity 500 fb^{-1} , for the heavy neutrinos with mass 150 GeV. We have adopted the efficiencies for the signal and the SM background found by the realistic Monte Carlo simulations in [25].

	Events before cuts	Events after cuts
FND (NH)	162	52.0
FND (IH)	3133	776.1
FD	133605	42671.3
SM background	5476408	10500
FND (NH, $\ell = \mu$)	1108	
FND (NH, $\ell = \tau$)	1160	
FND (IH, $\ell = \mu$)	1648	
FND (IH, $\ell = \tau$)	1655	

Table 4: The same as Table 3, but $\sqrt{s} = 1$ TeV.

In both $\sqrt{s} = 500$ GeV and 1 TeV, the signal to background ratio is large ($> 5 - \sigma$) for the FND (IH) and FD cases, while the significance is negligible for the FND (NH) case. If we naively expect a similar efficiency for the $\ell = \mu$ case, the heavy neutrinos can be observed with a large significance for both the FND and FD cases. In [25], the $\ell = \tau$ case is also analyzed

in detail. In this case, the signal $N \rightarrow \nu e W (W \rightarrow q\bar{q}')$ is considered as the background, and the analysis depends on the number of the signal events and hence, we cannot simply adopt the results in [25]. However, since the main backgrounds are $e\nu W \rightarrow e\nu q\bar{q}$ and $WW \rightarrow \ell\nu q\bar{q}'$ also for this case, we can expect that the efficiency for our case is similar to the one obtained in [25], which is roughly the same as in the $\ell = e$ case. Thus, we expect, for the $\ell = \tau$ case, a large significance for the signal events in both the FND and the FD cases.

5.3 Heavy neutrino signal with the general parameterization

In the general parameterization for the FND case, \mathcal{R} is a function of the Dirac phase (δ), the Majorana phase (ρ) and y in the general orthogonal matrix. In order to identify a region for these parameters satisfying the constraint on the ϵ -matrix, we perform a parameter scan by varying $-\pi \leq \delta, \rho \leq \pi$ with an interval of $\frac{\pi}{20}$ and $0 \leq y \leq 1$ with an interval of 0.02.² Then, for the identified parameters, we calculate the production cross section of the i -th generation heavy neutrino at the LHC through the process $q\bar{q}' \rightarrow \ell N_i$ ($u\bar{d} \rightarrow \ell_\alpha^+ N_i$ and $\bar{u}d \rightarrow \ell_\alpha^- \bar{N}_i$) given by

$$\sigma(q\bar{q}' \rightarrow \ell_\alpha N_i) = \sigma_{LHC} |\mathcal{R}_{\alpha i}(\delta, \rho, y)|^2, \quad (36)$$

where σ_{LHC} is the cross section given in Eq. (13). Similarly, the production cross section at the ILC is

$$\sigma(e^+ e^- \rightarrow \bar{\nu}_\alpha N_i) = \sigma_{ILC} |\mathcal{R}_{\alpha i}(\delta, \rho, y)|^2, \quad (37)$$

where σ_{ILC} is given in Eq. (15), and we have used the approximation $\mathcal{N}^\dagger \mathcal{R} \simeq U_{MNS}^\dagger \mathcal{R}$ because $|\epsilon_{\alpha\beta}| \ll 1$ as discussed in the previous section. The partial decay widths for the process $N_i \rightarrow \ell_\alpha^- W^+ / \nu_\alpha Z / \nu_\alpha h$ are obtained by multiplying Eq. (14) and the factor $|\mathcal{R}_{\alpha i}(\delta, \rho, y)|^2$ together.

Fig. (5) shows the results of the parameter scan for the heavy neutrino production cross section with the tri-lepton final states at the LHC. Each dots satisfies the experimental constraints on all the ϵ -matrix elements. The first (second) column shows the results for the NH (IH) case. In the first (second) row, the results are shown as a function of δ (y) for the final state with two electrons, while the corresponding results for the final state with two muons are shown in the third and forth rows. Comparing the results with those for the simple parameterizations, the signal cross sections for the NH case receive significant enhancements for a certain parameter set, while for the IH case, we only have an enhancement by a factor 2 – 4. The maximum signal

² The Dirac mass matrix elements grow exponentially as we raise $|y|$. For a value $y > 1$, the neutrino oscillation data are realized under the fine-tuning between the large elements. Although the neutrino oscillation data are correctly reproduced for any values of y in the general parameterization, we only consider $y \leq 1$ to avoid the fine-tuning.

	ee	$\mu\mu$
NH (fb)	0.515	5.95
IH (fb)	0.575	0.475

Table 5: The maximum LHC cross sections for the final states with two electrons and two muons ,respectively, at the LHC with $\sqrt{s} = 14$ TeV.

	NH (fb)	IH (fb)
$\ell = e$	8.5	8.5
$\ell = \mu$	130	11.0

Table 6: The maximum cross sections at the ILC with $\sqrt{s} = 500$ GeV. Here we have fixed the heavy neutrino mass to be 150 GeV. Each dots satisfies the experimental constraints on all the ϵ -matrix elements. The first (second) column shows the results for the NH (IH) case. The first and second rows correspond to the results for the case of $\ell = e$, while the corresponding results for the case of $\ell = \mu$ are shown in the third and forth rows.

cross sections we can achieve in the general parameterization are listed on Table 5. Interestingly, the maximum cross section for the NH case with the final state including two muons can even be larger than the one for the FD case.

Fig. 6 shows the cross section for the process $e^+e^- \rightarrow \nu N$, followed by the decays $N \rightarrow \ell W$ and $W \rightarrow q\bar{q}'$, at the ILC with $\sqrt{s} = 500$ GeV. Here we have fixed the heavy neutrino mass to be 150 GeV. Each dots satisfies the experimental constraints on all the ϵ -matrix elements. The first (second) column shows the results for the NH (IH) case. In the first (second) row, the results are shown as a function of δ (y) for the case of $\ell = e$, while the corresponding results for the case of $\ell = \mu$ are shown in the third and forth rows. Similarly to the LHC results, we have found the significant enhancements for the NH case compared with the results for the simple parameterizations, while we have no significant enhancement for the IH case. The maximum signal cross sections we can achieve in the general parameterization are listed on Table 6. The maximum cross section for the NH case with $\ell = \mu$ can even be larger than the one for the FD case. We have performed the same analysis also for the ILC with $\sqrt{s} = 1$ TeV. The maximum signal cross sections in this case are listed on Table 7. We have about a 30 – 40 % enhancement in the cross sections by the increase of the collider energy.

The main backgrounds are $e\nu W \rightarrow e\nu q\bar{q}$ and $WW \rightarrow \ell\nu q\bar{q}$, which are dramatically reduced by the selection using an isolated-electron track with a requirement of its energy range, $10 \text{ GeV} \leq E_e \leq 200 \text{ GeV}$, the requirement of the reconstructed di-jet mass to be consistent with W hypothesis etc (see [25] for details). The Maximum signal cross section for $\sqrt{s} = 1$ TeV and the same luminosity $\mathcal{L} = 500 \text{ fb}^{-1}$ are listed on Table 7. We have only listed $e+jj$ and $\mu+jj$

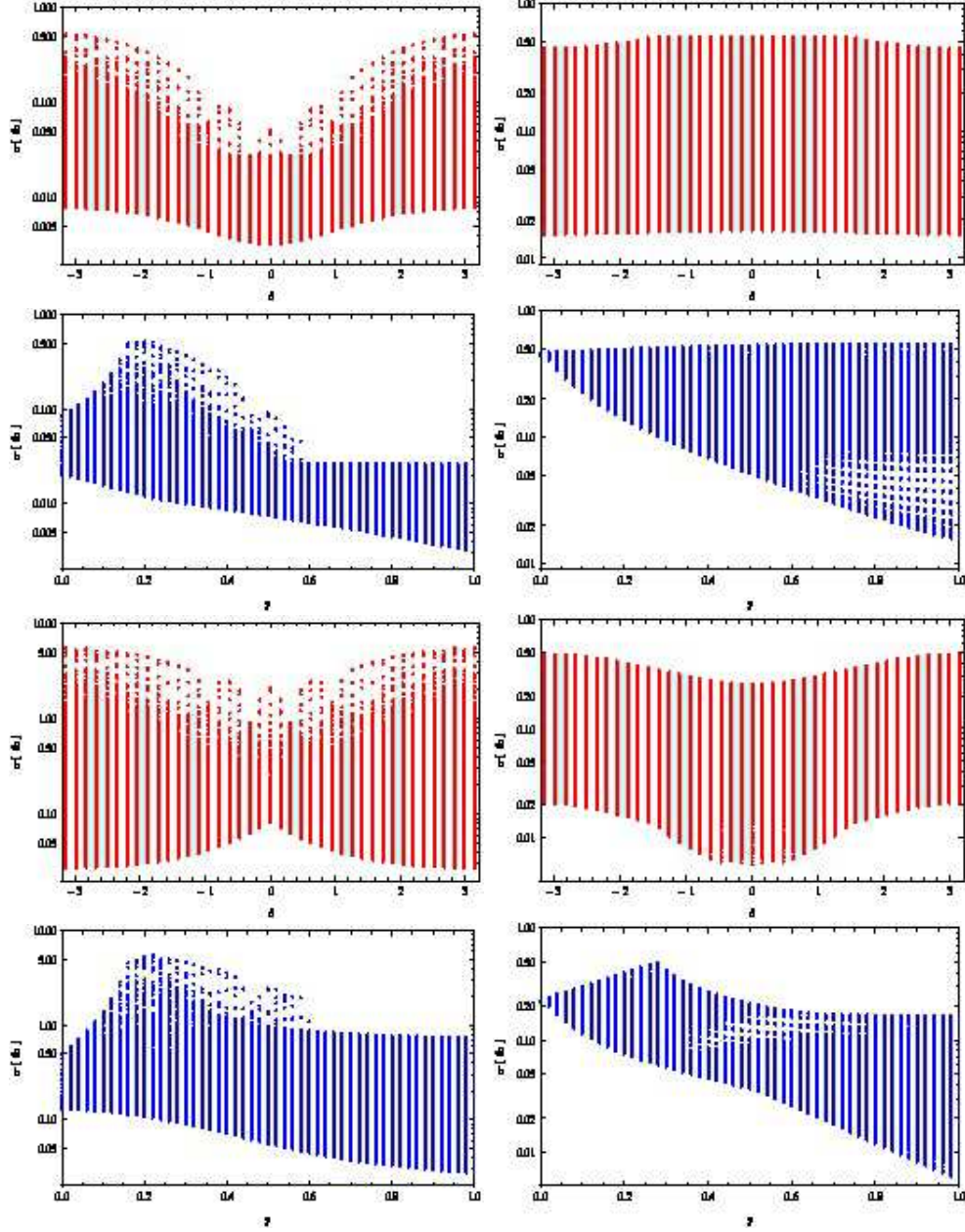


Figure 5: Signal cross sections providing the tri-lepton final states as function of the Dirac phase (δ) and γ for the heavy neutrino mass of 100 GeV, at the LHC with $\sqrt{s} = 14$ TeV. Each dot satisfies the experimental constraints on all the elements in the ϵ -matrix. The first (second) column corresponds to the results for the NH (IH) case. The first two rows are for the final states with two electrons, while the last two rows are for the final states with two muons.

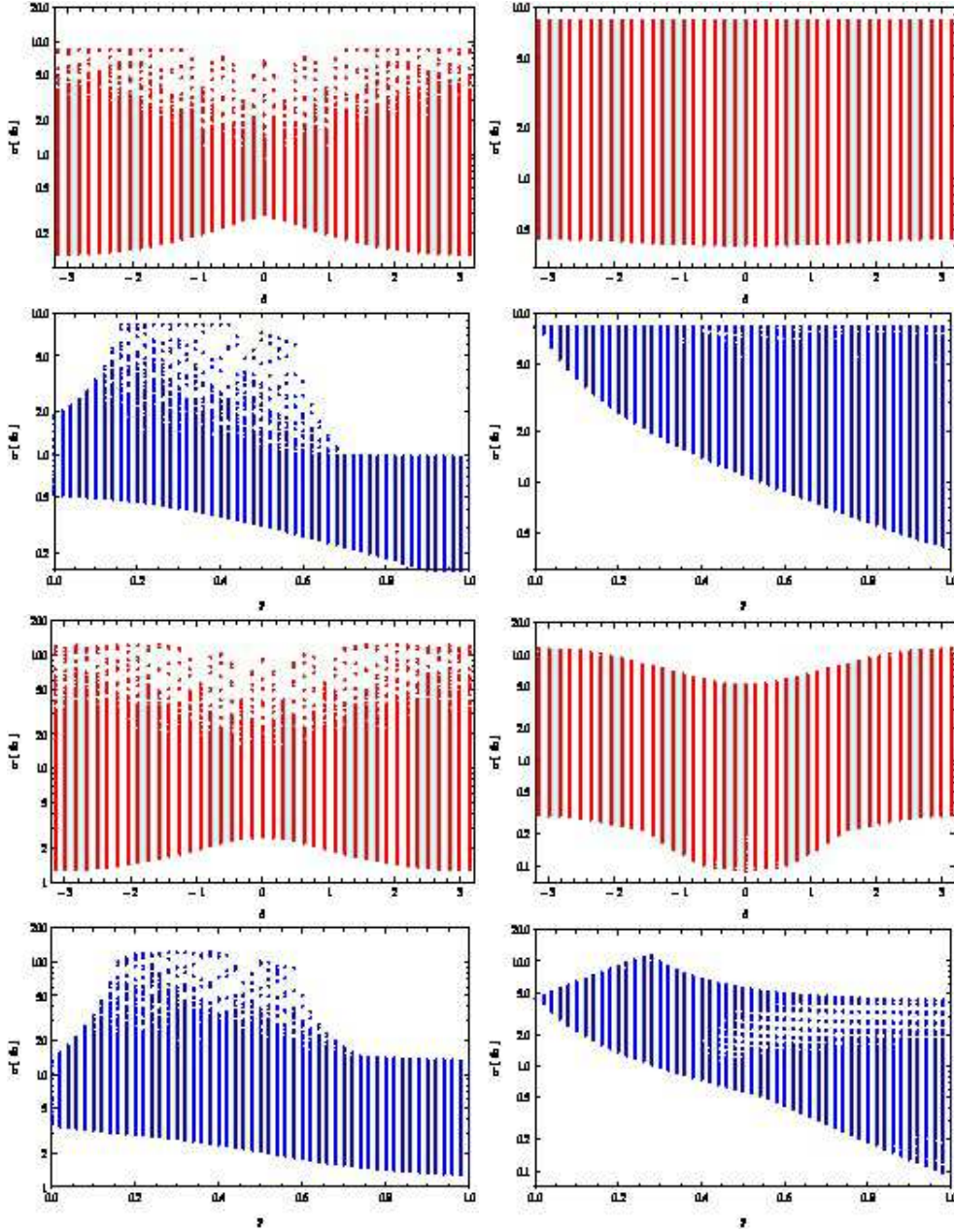


Figure 6: The production cross sections for the process $e^+e^- \rightarrow \nu N$, followed by the decays $N \rightarrow \ell W$ ($\ell = e, \mu$) and $W \rightarrow q\bar{q}'$, as functions of the Dirac phase(δ) and y , at the ILC with $\sqrt{s} = 500$ GeV. Here we have fixed the heavy neutrino mass to be 150 GeV. Each dot satisfies the experimental constraints on all the ϵ -matrix elements. The first (second) column shows the results for the NH (IH) case. In the first (second) row, the results are shown as a function of δ (y) for the case of $\ell = e$, while the corresponding results for the case of $\ell = \mu$ are shown in the third and fourth rows.

	NH (fb)	IH (fb)
$\ell = e$	11.0	11.0
$\ell = \mu$	180	180

Table 7: The same as Table 6, but for $\sqrt{s} = 1$ TeV.

signal cross section as functions of δ , ρ and y .

From Tables 6 and 7 the signal cross sections for $\mu+jj$ in NH dominates over IH by an order of magnitude for both the collider energies, $\sqrt{s} = 500\text{GeV}$ and $\sqrt{s} = 1$ TeV. The signal cross sections for $e+jj$ in NH is almost the same as that in the IH case for both the collider energies, $\sqrt{s} = 500\text{GeV}$ and $\sqrt{s} = 1$ TeV. The $\mu\mu$ case cross sections at $\sqrt{s} = 500\text{GeV}$ and $\sqrt{s} = 1$ TeV are some factors greater than the FD cases respectively.

6 Conclusions

We have studied the inverse seesaw scenario and the signature of the pseudo-Dirac heavy neutrino production at the LHC and ILC. In the inverse seesaw scenario, the light neutrino masses are realized by small lepton-number-violating parameters and hence the SM singlet neutrinos have sizable Dirac Yukawa couplings with the SM lepton doublets and Higgs doublet even for their mass scale being at the TeV scale or smaller. As a result, the heavy neutrinos can be produced at the LHC and ILC. Based on a concrete model realizing the inverse seesaw in the context of the NMSSM, we have fixed the model parameters so as to satisfy the experimental results such as the neutrino oscillation data, the precision measurements of the weak boson decays, and the lepton-flavor-violating decays of charged leptons. We have considered two typical cases for the neutrino flavor structures of the model, namely, the FND and FD cases. With the fixed parameters, we have calculated the production cross sections of the heavy neutrinos at the LHC and ILC.

First we have considered simple parameterizations with all zero CP-phases. For the LHC with $\sqrt{s} = 14$ TeV, we have analyzed the productions of the heavy neutrinos with a degenerate 100 GeV mass, providing the tri-lepton final states with the like-sign electrons or muons. After imposing suitable cuts, we have found that the $5 - \sigma$ statistical significance of the signal events over the SM background can be achieved for the luminosity around 11 fb^{-1} in the FD case. On the other hand, the production cross sections in the FND case is too small to observe the heavy neutrino signal.

We have also studied the heavy neutrino production at the ILC with $\sqrt{s} = 500 \text{ GeV} - 1 \text{ TeV}$, where the final state with a single, isolated electron, and di-jet and large missing energy is

considered. For the luminosity $\sqrt{s} = 500 \text{ fb}^{-1}$, we can obtain clear signatures of the heavy neutrinos with mass 150 GeV for the IH mass spectrum in the FND case and the FD case. On the other hand, the significance for the NH mass spectrum in the FND case has been found to be low. Since we can expect the similar efficiencies of the signal and SM background for the final states with different lepton flavors, muon or tau, the heavy neutrinos can be detected with a large statistical significance in the modes for all FND and FD cases.

For completeness, we have also considered the general parameterization for the Dirac neutrino mass matrix by introducing a general orthogonal matrix and CP-phases, for the FND case. In this case, three new parameters, the Dirac CP-phase (δ), the Majorana CP-phase (ρ) and one angle of the orthogonal matrix, are newly involved in our analysis. We have performed a parameter scan and identified the parameter region which satisfies all experimental constraints on the elements of the ϵ -matrix. Then, we have shown the signal cross sections of the heavy neutrino production for the parameters identified. For both the LHC and ILC cases, we have found significant enhancements of the cross section for the NH case and the resultant cross section can be of the same order of the FD case. On the other hand, such a remarkable enhancement has not been observed for the IH case.

If the heavy neutrinos are discovered in the future, this indicates that a mechanism of the neutrino mass generation is not due to the conventional seesaw mechanism, because the expected cross section for the conventional seesaw is extremely small. In addition, the flavor dependent signal events from the heavy neutrino productions provide us with valuable information to investigate the flavor structure of the model for the neutrino mass generation.

Finally we comment on the current bound of the heavy neutrino production at the LHC. The ATLAS experiment [27] has reported their results on the search for the heavy neutrinos based on the production through effective four-fermion operators [28]. The vector operator of $(\bar{d}\gamma^\mu u)(\bar{N}\gamma_\mu \ell)/\Lambda^2$ is relevant to our case. The final states with $\ell\ell jj$ ($\ell = e$ or μ) have been analyzed as a signal of the heavy neutrino production, followed by the decay $N \rightarrow \ell W$, $W \rightarrow jj$. From the data corresponding to an integrated luminosity of 2.1 fb^{-1} at $\sqrt{s} = 7 \text{ TeV}$, the ATLAS experiment has set the lower bound on the cutoff scale Λ as a function of the heavy neutrino mass $\geq 200 \text{ GeV}$. For example, it is found that $\Lambda \geq 2.8 \text{ TeV}$ for $M = 200 \text{ GeV}$. We interpret this result to the upper bound on the heavy neutrino production cross section through the four-fermion operator as $\sigma(q\bar{q}' \rightarrow \ell N) \leq 24.0 \text{ fb}$. In the FD case, we find $\sigma(q\bar{q}' \rightarrow \ell N) \simeq 3.77 \text{ fb}$ and therefore, the parameter region we have examined in this paper is consistent with the current LHC results.

Acknowledgments

A.D. would like to thank Joydeep Chakrabortty, Partha Konar and Srubabati Goswami for useful discussions and comments. He would also like to thank PRL, Ahmedabad for their hospitality when a part of the work is done. This visit is supported by APS-IUSSTF Physics Student Visitation Program. The work of N.O. is supported in part by the DOE Grants, No. DE-FG02-10ER41714.

References

- [1] K. Nakamura *et al.* [Particle Data Group Collaboration], J. Phys. G **37**, 075021 (2010).
- [2] K. Abe *et al.* [T2K Collaboration] Phys. Rev. Lett. **107**, 041801 (2011).
- [3] P. Adamson *et al.* [MINOS Collaboration], Phys. Rev. Lett. **107**, 181802 (2011).
- [4] Y. Abe *et al.* [DOUBLE-CHOOZ Collaboration], Phys. Rev. Lett. **108**, 131801 (2012).
- [5] F. P. An *et al.* [DAYA-BAY Collaboration], Phys. Rev. Lett. **108**, 171803 (2012).
- [6] J. K. Ahn *et al.* [RENO Collaboration], Phys. Rev. Lett. **108**, 191802 (2012).
- [7] P. Minkowski, Phys. Lett. B **67**, 421 (1977); T. Yanagida, in *Proceedings of the Workshop on the Unified Theory and the Baryon Number in the Universe* (O. Sawada and A. Sugamoto, eds.), KEK, Tsukuba, Japan, 1979, p. 95; M. Gell-Mann, P. Ramond, and R. Slansky, *Supergravity* (P. van Nieuwenhuizen *et al.* eds.), North Holland, Amsterdam, 1979, p. 315; S. L. Glashow, *The future of elementary particle physics*, in *Proceedings of the 1979 Cargèse Summer Institute on Quarks and Leptons* (M. Levy *et al.* eds.), Plenum Press, New York, 1980, p. 687; R. N. Mohapatra and G. Senjanovic, Phys. Rev. Lett. **44**, 912 (1980).
- [8] R. N. Mohapatra, Phys. Rev. Lett. **56** (1986) 561; R. N. Mohapatra and J. W. F. Valle, Phys. Rev. D **34**, 1642 (1986).
- [9] I. Gogoladze, N. Okada and Q. Shafi, Phys. Lett. B **672**, 235 (2009).
- [10] P. Fayet, Nucl. Phys. **B 90** (1975) 104; H. P. Nilles, M. Srednicki and D. Wyler, Phys. Lett. **B 120** (1983) 346; J. P. Derendinger and C. A. Savoy, Nucl. Phys. **B 237** (1984) 307; J. Ellis, J. F. Gunion, H. E. Haber, L. Roszkowski and F. Zwirner, Phys. Rev. **D 39** (1989) 844; L. Durand and J. L. Lopez, Phys. Lett. **B 217** (1989) 463; M. Drees, Int. J. Mod. Phys. **A 4** (1989) 3635.

- [11] A. Broncano, M. B. Gavela and E. E. Jenkins, Phys. Lett. B **552**, 177 (2003) [Erratum-ibid. B **636**, 330 (2006)]; Nucl. Phys. B **672**, 163 (2003).
- [12] J. Pumplin, D. R. Stump, J. Huston, H. L. Lai, P. Nadolsky and W. K. Tung, JHEP **07** (2002) 012.
- [13] G. Aad et al. [ATLAS Collaboration], Phys. Lett. B **716**, 1 (2012)
- [14] S. Chatrchyan et al. [CMS Collaboration], Phys. Lett. B **716**, 30 (2012)
- [15] S. Antusch, C. Biggio, E. Fernandez-Martinez, M. B. Gavela and J. Lopez-Pavon, JHEP **0610**, 084 (2006).
- [16] A. Abada, C. Biggio, F. Bonnet, M. B. Gavela and T. Hambye, JHEP **0712**, 061 (2007).
- [17] A. Ibarra, E. Molinaro and S. T. Petcov, JHEP **1009**, 108 (2010); Phys. Rev. D **84**, 013005 (2011); D. N. Dinh, A. Ibarra, E. Molinaro and S. T. Petcov, JHEP **1208**, 125 (2012) [Erratum-ibid. **1309**, 023 (2013)].
- [18] J. Adam et. al. [MEG Collaboration], Phys. Rev. Lett. **107**,171801, (2011).
- [19] B. Aubert et. al. [BABAR Collaboration], Phys. Rev. Lett. **104**,021802,(2010).
- [20] See, for summary, B. O' Leary et. al. [SuperB Collaboration], arXiv: 1008.1541[hep-ex].
- [21] F. del Aguila and J. A. Aguilar-Saavedra, Nucl. Phys. B **813**, 22 (2009); Phys. Lett. B **672**, 158 (2009).
- [22] M. Hirsch, F. Staub and A. Vicente, Phys. Rev. D **85**, 113013 (2012).
- [23] A. Abada, D. Das, A. Vicente and C. Weiland, JHEP **09** (2012)015.
- [24] C. Y. Chen and P. S. B. Dev, Phys. Rev. D **85**, 093018 (2012).
- [25] T. Saito, M. Asano, K. Fujii, N. Haba, S. Matsumoto, T. Nabeshima, Y. Takubo and H. Yamamoto *et al.*, Phys. Rev. D **82**, 093004 (2010).
- [26] N. Haba, S. Matsumoto and K. Yoshioka, Phys. Lett. B **677**, 291 (2009).
- [27] G. Aad *et al.* [ATLAS Collaboration], Eur. Phys. J. C **72**, 2056 (2012).
- [28] F. del Aguila, S. Bar-Shalom, A. Soni and J. Wudka, Phys. Lett. B **670** (2009) 399.